Available online at www.sciencedirect.com

SciVerse ScienceDirect

Journal of the European Ceramic Society 32 (2012) 1795–1802

www.elsevier.com/locate/jeurceramsoc

Effect of solid solution formation on densification of hot-pressed ZrC ceramics with MC (M = V, Nb, and Ta) additions

Xin-Gang Wang [a], Ji-Xuan Liu [a,b], Yan-Mei Kan [a], Guo-Jun Zhang [a,*]

[a] *State Key Laboratory of High Performance Ceramics and Superfine Microstructures, Shanghai Institute of Ceramics, Shanghai 200050, China*
[b] *Graduate School of the Chinese Academy of Sciences, Beijing 100049, China*

Received 23 April 2011; received in revised form 20 October 2011; accepted 29 October 2011
Available online 14 January 2012

Abstract

ZrC ceramics with additions of MC (M = V, Nb, and Ta) were prepared by hot pressing, and the effect of MC additions on densification was analyzed in terms of the solubility limit and kinetics of formation of MC solid solutions with ZrC. VC additions of 2.5–10 vol% (3.5–13.5 mol%), which is higher than its solid solubility limit of 1.3 vol% (1.8 mol%), effectively promoted the densification process and nearly fully dense ZrC ceramics were obtained by hot-pressing at 1900 °C. In contrast, both NbC and TaC additions, which can form unlimited solid solutions with ZrC, have no obvious contribution to ZrC densification. This is because formation of the solid solution of NbC and TaC with ZrC matrix requires higher temperature and longer time due to their stronger bonding energy, compared to VC. SEM observation demonstrated that the VC addition resulted in larger grains, compared to ZrC ceramics with NbC and TaC additions.

Keywords: Hot pressing; Sintering; Carbides; Solid solution; Structural applications

1. Introduction

The refractory carbides of group IV–V transition metals, such as ZrC, HfC and TaC, comprise a family of materials, which have the NaCl crystal structure. ZrC has a unique combination of properties, including a very high melting point (>3540 °C), low density, high hardness, good thermal shock resistance and low chemical reactivity.[1,2] As a result, ZrC is a potential candidate for applications such as next-generation rocket engines and hypersonic spacecraft working at 2200–3000 °C.[3] In addition, ZrC has low neutron absorption cross-section and resistance to the corrosion of nuclear fission products.[4,5] In the framework of the Generation-IV international project, ZrC is one of the promising inert matrix materials to be used for some fuel components of high temperature nuclear reactors such as the gas-cooled fast reactor and high temperature gas reactor.[6–8]

As with other ultra-high temperature ceramics, such as ZrB_2, HfB_2 and HfC, owing to the strong covalent bonding and low self-diffusion coefficient, very high temperature (2300–2600 °C) and external pressure are required to densify ZrC ceramics.[9–11] Besides the sintering temperature, time and pressure, the densification of ZrC is also affected by the character of the ZrC powders used, including (1) purity, particle size and particle distribution of the raw ZrC powders; (2) additives; and (3) carbon vacancies or oxygen atom substitution onto the carbon sites. Zirconium carbide can be a non-stoichiometric compound ZrC_{1-x} with the C/Zr ratio ranging from 0.493 to 1. The sintering activation energy of ZrC_{1-x} decreases with increase of x value. For example, the relative density of the ZrC_{1-x} ceramics hot-pressed at 2300 °C for 5 min increased from 91% to 97.8% when the x value increased from 0 to 0.35.[11] This is because the increase in carbon deficiency in the ZrC_{1-x} lattice enhanced the mass transport and consequently the densification was accelerated.[12,13] Meanwhile, the intergranular glide and dislocation motion caused by the external applied loads can also contribute to the densification. Gendre et al. studied densification mechanism of $ZrC_{0.94}O_{0.05}$ powders by spark plasma sintering under several applied loads (25, 50, 100 MPa) and revealed that at a low macroscopic applied stress (25 MPa), an intergranular glide mechanism dominates the densification process, while dislocation motion happened at a higher applied load (100 MPa).[14] Reductive additives such as B, C and B_4C can act as densification

* Corresponding author. Tel.: +86 21 52411080; fax: +86 21 52413122.
E-mail address: gjzhang@mail.sic.ac.cn (G.-J. Zhang).

0955-2219/$ – see front matter © 2011 Elsevier Ltd. All rights reserved.
doi:10.1016/j.jeurceramsoc.2011.10.045

aids to remove the oxide impurities present on the surface of the ZrC_{1-x} particles to activate the densification.[12,15,16] Other additives, like Mo and $MoSi_2$ promoted the densification by a liquid phase formation.[2,17]

In addition, solid solution formation also can promote densification by enhancing mass transport. Huang et al. reported that addition of VC in WC can promote the densification due to formation of the (V,W)C solid solution.[18] Hu et al. reported that the addition of $TaSi_2$ contributed to the densification of ZrB_2–SiC and HfB_2–SiC composites. A probable reason is that Ta atoms from the decomposition of $TaSi_2$ dissolve into boride grains and cause the decrease of the activation energy for diffusion at boride grain boundaries.[19] MC (M = V, Nb, and Ta) have high melting points and the same crystal structure as ZrC. Because the difference in covalent radii between Zr (1.597 Å) and V (1.338 Å) exceeds 15%, VC forms a limited solid solution with ZrC. As the covalent radius of Nb and Ta was 1.456 Å and 1.457 Å, respectively, a smaller radius difference (<15%) between Nb, Ta and Zr leads to a continuous solid solution of Nb and Ta carbides with ZrC.[20] The phase diagrams of ZrC–VC, ZrC–NbC and ZrC–TaC systems as shown in Fig. 1 demonstrate this tendency.[21]

The aim of the present work is to investigate the effects of MC (M = V, Nb, and Ta) additives, which have different solid solubilities and dissolution kinetics in ZrC, on the densification and microstructural evolution of ZrC ceramics.

2. Experimental procedure

2.1. ZrC Powder synthesis

ZrC powder was synthesized by carbothermal reaction between ZrO_2 and C at 1700 °C in vacuum. The starting powders were ZrO_2 and graphite powders and their impurity content, average particle size and suppliers are listed in Table 1. The ZrO_2 and graphite powders with the molar ratio of 1:3 according to Eq. (1) were ball mixed with ethanol in a plastic bottle for 24 h using ZrO_2 media (12 mm in diameter).

$$ZrO_2 + 3C = ZrC + 2CO(g) \quad (1)$$

After mixing, the slurries were dried in a rotary evaporator at 70 °C, and then the dried powder mixtures were pressed into pellets with dimensions of 30 mm × 37 mm × 5 mm under a pressure of 0.1 MPa to improve particle contact for promoting solid state reaction at high temperature. Several pellets (50 g batches) were then placed into a graphite crucible and heated to 1700 °C for 1 h in a graphite resistance furnace (ZT-18-22, Shanghai Chenhua Electrical Furnace Inc., Shanghai, China). The total pressure in the furnace chamber was kept below 5 Pa by a vacuum pump. After the reaction, the furnace was cooled down to room temperature naturally. The reacted pellets were crushed to powder in an agate mortar and then sieved through a 200-mesh screen. The produced ZrC had 99% purity and an average particle size of 1–3 μm. The oxygen content of the as-synthesized ZrC powder was determined by Oxygen-Azote mensuration equipment (TC600, LECO, USA). VC, NbC and TaC (99% purity, 2–5 μm, Beijing Mountai Technical Development Center for non-ferrous Metals, Beijing, China) were used as additives.

2.2. Sample preparation

The synthesized ZrC powder and designated amount (1–10 vol%) of MC additives were mixed by ball milling in ethanol in a plastic bottle for 24 h using Si_3N_4 media with a diameter of 10 mm. The weight ratio of the powders to the Si_3N_4 media was 1:3. After mixing, the slurry was dried at 70 °C using a rotary evaporator. The dried powder mixture cakes were sieved through a 200-mesh screen to form granules. The granules of ZrC powder, with or without additives, were compacted in a graphite die lined with a graphite foil coated with BN. The powder compacts were heated at 10 °C/min to 1450 °C and held for 30 min under a mild vacuum (<10 Pa) for out-gassing. After out-gassing, the furnace atmosphere was switched to flowing argon (>10^5 Pa). In order to densify the powder compacts of ZrC powder, with or without additives, the compacts in the graphite die were subjected to a uniaxial pressure of 30 MPa and were heated at the same rate to the designed densification temperatures ranging from 1800 °C to 2000 °C with 100 °C intervals. The compacts were sintered at the densification temperatures for 1 h. At the end of the holding time, the furnace was cooled at a rate of 30 °C/min to 1700 °C, then the applied pressure was removed, after which the furnace was cooled naturally to room temperature. The produced specimens had dimensions of 37 mm × 30 mm × 5 mm.

2.3. Characterization

The bulk densities of the sintered ZrC ceramics were measured using the Archimedes method. The relative densities were calculated by dividing the measured bulk density by the appropriate calculated theoretical density that was based on the composition. The phase present was determined by X-ray diffraction (XRD, *D*/max 2550 V, Tokyo, Japan). The lattice parameters were determined by XRD using a Guinier–Hägg focusing camera (XCD-1000, Sweden) with $CuK_{\alpha 1}$ (λ = 1.5405981 Å) radiation. Si powder (99.99% purity) was used as an internal standard. The obtained photographs were evaluated with a computerized scanner system.[22] The lattice parameter of each sample was determined by means of the PIRUM program based on Guinier–Hägg film data.[23] The amount of MC dissolved in ZrC to form solid solution was determined by Vegard's law (a linear relation), which is based on the assumption of an ideal crystal structure. Secondary electron images of fracture surfaces and acid etched polished surfaces were taken by scanning electron microscopy (SEM, Hitachi S-570, Tokyo, Japan). The chemical composition and backscattered electron (BSE) image of the hot-pressed specimens were analyzed using electron probe microanalyzer (JEOL JXA-8100F, Japan) along with energy-dispersive spectroscopy (EDS, Oxford INCA energy). Some hot-pressed samples were ground and polished with a diamond paste to 0.5 μm and chemically etched using an acid mixture of HF: HNO_3: H_2O (volume ratio = 1:1:2) for microstructural investigation. The

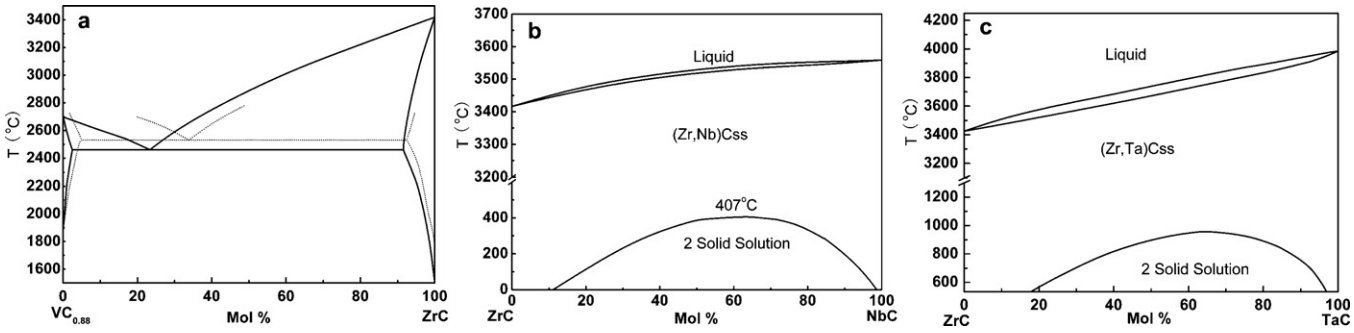

Fig. 1. Phase diagrams of (a) ZrC–VC (No. 09033), (b) ZrC–NbC (No. 09033), and (c) ZrC–TaC (No. 09025) systems.[21]

Table 1
Main characteristics of the starting powders.

Powder	Supplier	Variety	Particle size (μm)	Purity (%)
ZrO_2	Dongguan CSG Ceramics Technology CO., LTD China	Monolithic	0.2	>99%, Hf < 0.5%
Carbon	Shanghai Colloidal Graphite Company, China	Graphite	1.5	99%

average grain sizes of the sintered ZrC ceramics were determined using Image Pro-plus 5.0 software (Media Cybernetics) on the acid etched polished surfaces.

3. Results and discussion

3.1. Densification

Fig. 2 compares the relative density of the sintered pure ZrC and the ZrC with additions of 10 vol% VC, NbC and TaC. The relative density of the pure ZrC ceramics sintered at 1900 °C and 2000 °C was 80% and 92%, respectively. The ZrC ceramics with 10 vol% VC addition reached a relative density of 98% after sintering at 1900 °C. However, the relative density of the ZrC with 10 vol% NbC and TaC sintered at 2000 °C was only 95.1% and 90.7%, respectively. Compared with NbC and TaC additions, VC was the most effective sintering aid for the ZrC powder.

In order to investigate the effects of the quantity of VC on the densification of ZrC, ZrC with 1.0, 2.5, and 5.0 vol% VC additions were hot-pressed at temperatures of 1800 °C, 1900 °C and 2000 °C. The relative density of ZrC as a function of VC content is shown in Fig. 3. As can be seen from this figure, the relative density of the ZrC hot-pressed at 1800 °C increased markedly with the increase in VC content. The relative density of ZrC sintered at 1900 °C increased from 86% for 1.0 vol% VC addition to 98% for 2.5 vol% VC. As VC content increased up to 2.5 vol% or higher, the relative density had no further increase. The effect of different MC additives and content on ZrC densification was analyzed by means of phase identification and solid solution formation, as described in the following sections.

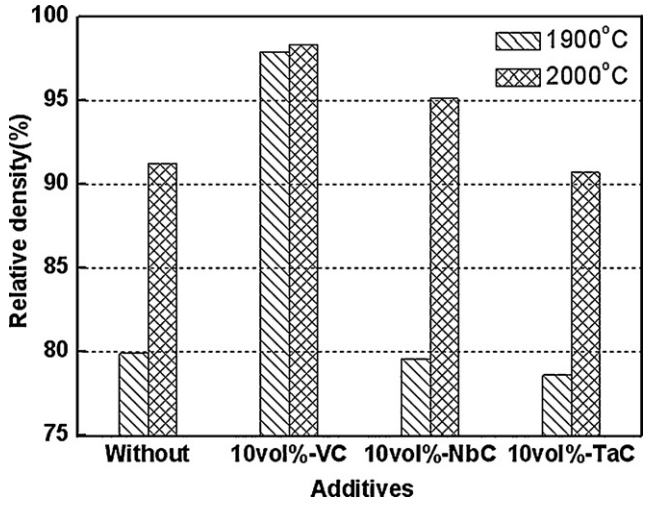

Fig. 2. Relative density of pure ZrC and with addition of 10 vol% VC, NbC and TaC sintered at 1900–2000 °C.

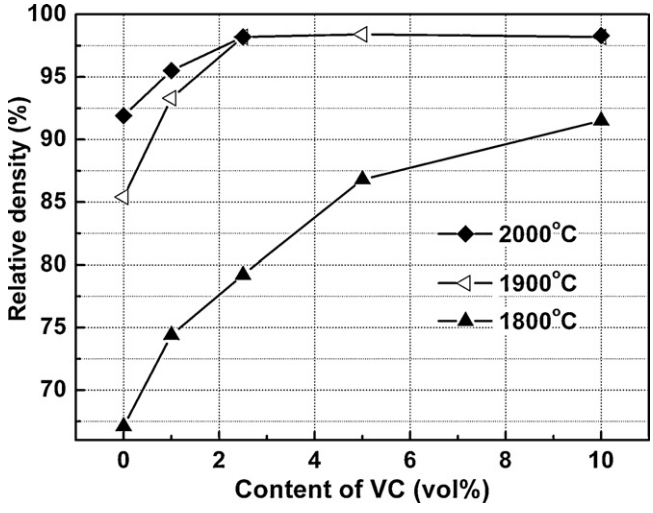

Fig. 3. Relative density of ZrC sintered at different temperatures as a function of VC content.

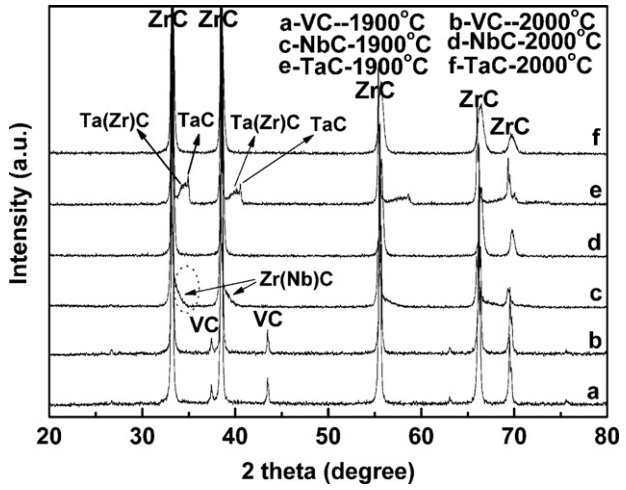

Fig. 4. XRD patterns of ZrC with MC (M = V, Nb, Ta) additives sintered at different temperature. (e) The peaks broadening shows the formation of Ta(Zr)C solid solution.

3.2. Solid solution formation

XRD patterns of the ZrC samples without and with 10 vol% MC additions hot pressed at 1900 °C and 2000 °C are shown in Fig. 4. As seen from Fig. 4b, d and f, VC phase exists in the 10 vol% VC added ZrC ceramics sintered at 2000 °C for 1 h, while NbC and TaC phases are not found in the XRD patterns of the ZrC with 10 vol% NbC and TaC sintered at 2000 °C (Fig. 4d and f), respectively. The enlarged XRD patterns of the ZrC with and without additive sintered at 2000 °C (shown in Fig. 5) indicate that the ZrC (1 1 1) peak for ZrC with 10 vol% VC sample (Fig. 5b) shifts towards higher 2θ angles, compared with the pure ZrC (Fig. 5a). Considering the VC phase is still present (see Fig. 4b), this is evidence that a certain amount of VC dissolved in ZrC to form a limited solid solution, as shown in the ZrC–VC phase diagram. Similar phenomena (peaks shift) were observed in the ZrC–10 vol% NbC and ZrC–10 vol% TaC

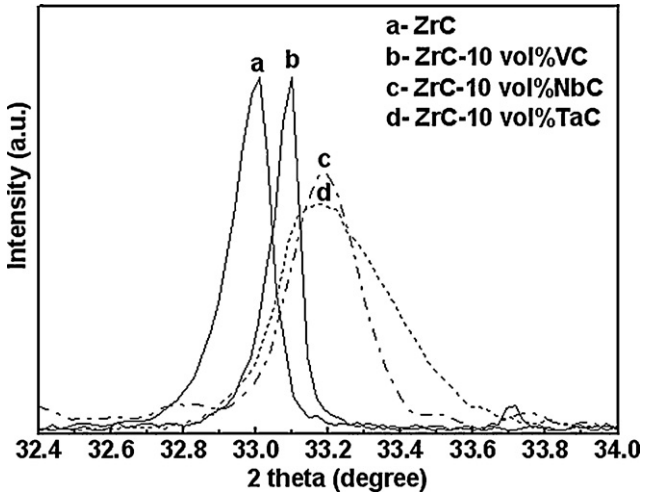

Fig. 5. Enlarged XRD patterns from a Guinier–Hägg camera between 32° and 34° (reflexion 1 1 1) for ZrC without and with MC (M = V, Nb, Ta) additives sintered at 2000 °C.

specimens (Fig. 5c and d) sintered at 2000 °C, indicating the formation of unlimited solid solution. As well as the dissolution of V, Nb, Ta in the ZrC lattice causing the shift of XRD patterns, the substitution of carbon by oxygen may also have contributed to the diffraction peaks shift, since the atomic radius of oxygen (0.66 Å) is smaller than that of carbon (0.76 Å), as Mathieu et al. reported.[14] In the present study, the ZrC ceramics with and without additive contain about the same content of oxygen impurity (0.74 ± 0.03 wt%) in raw powders. As the analysis of ZrC (1 1 1) peak shift on the ZrC with MC addition is based on the pure ZrC, and the ZrC with NbC and TaC addition hot pressed at 1900 °C did not have any densification, the possible oxygen dissolution in ZrC formula was neglected.

XRD results showed that ZrC formed limited solid solution with VC, and formed unlimited solid solution with NbC, which was further confirmed by EDS analysis. The BSE image of the polished surface of ZrC ceramics with 10vol%VC addition sintered at 2000 °C is shown in Fig. 6, in which the dark phase was identified as VC, and the light phase as ZrC matrix. Meanwhile, about 1.1 atomic% of V dissolved in ZrC, and the second phase of VC, also dissolves trace amounts of Zr (about 3.3 atomic%). Although the element concentration in EDS analysis was qualitative, the above results still indicate that only part of the VC dissolved in the ZrC matrix. On the other hand, EDS analysis of ZrC with 10 vol% NbC ceramics sintered at 2000 °C (not shown here) confirmed that the distribution of Nb element in ZrC was homogeneous. The NbC additive formed solid solution with ZrC, which was in agreement with the XRD results.

Based on the XRD and EDS analysis reported above, MC additives formed different solid solutions with ZrC, and their solid solution formation temperature was also different. All of the ZrC peaks in the XRD pattern of ZrC with 10 vol% NbC addition sintered at 1900 °C (Fig. 4c) are wider than the corresponding ZrC peaks of the same material sintered at 2000 °C (Fig. 4d). This peak broadening is the result of the overlapping of a series of peaks corresponding to different compositions of Zr(Nb)C solid solution at 1900 °C, i.e. the formed Zr(Nb)C solid solution was inhomogeneous in composition at 1900 °C for 1 h holding time. When the sintering temperature was increased to 2000 °C, the atom diffusion prompted the formation of a homogeneous Zr(Nb)C solid solution and, therefore, the broadening of the peaks disappeared. It can be concluded that the solid solution of NbC with ZrC started at 1900 °C. In the XRD pattern of ZrC with 10 vol% TaC sample, the peaks of TaC and Ta(Zr)C were observed (Fig. 4e) at 1900 °C, and disappeared after hot-pressing at 2000 °C (Fig. 4f). The formation of Ta(Zr)C solid solution at 1900 °C was caused by the diffusion of Zr into the TaC lattice. The Ta(Zr)C peaks disappeared at 2000 °C, which means a homogeneous Zr(Ta)C formed at 2000 °C. The above results testify that a higher temperature is required to form TaC–ZrC solid solution, compared with VC and NbC. This is because the kinetic rate of the TaC–ZrC solid solution formation was the lowest among the three MC additives, even though the equilibrium phase diagram (Fig. 1b and c) shows that NbC and TaC could form unlimited solid solutions with ZrC over 400 °C and 1000 °C, respectively.

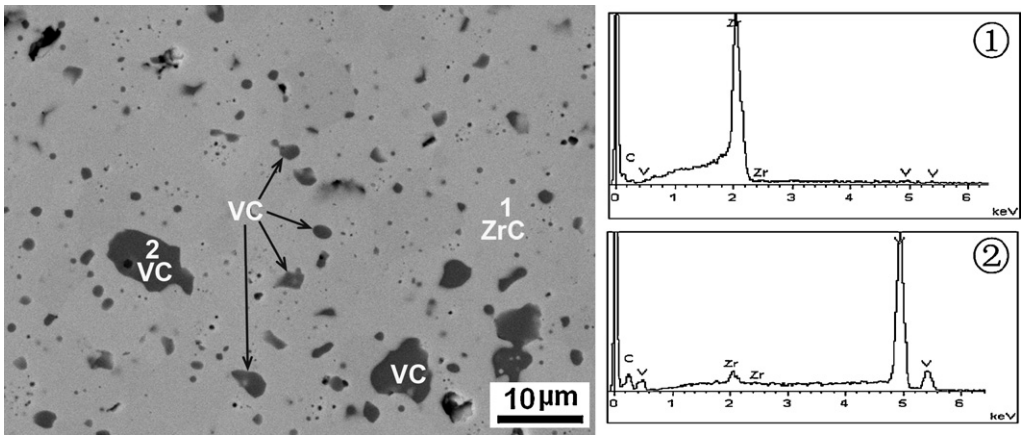

Fig. 6. Backscattered image of ZrC with 10 vol% VC sintered at 2000 °C and the EDS analysis results.

In order to confirm the solid solubility of the different MC additives in ZrC, lattice parameters of ZrC with various MC additives sintered at different temperatures were determined. According to the theoretical calculations,[20,24] ordered solid solution Zr_2C, Zr_3C, Zr_6C_5 may exist in ZrC_x at the carbon content x in the range of 0.47–0.54, 0.60–0.71, and 0.76–0.92, respectively. In the present study, the C/Zr ratio in the ZrC raw powder mixture was kept about 1:1, which is not in the theoretical range of the ordered solid solution formation. In addition, the XRD results of the ZrC with different additives did not reveal any existence of the ordered solid solutions such as Zr_6C_5, therefore, Vegard's law (a linear relation) based on identical crystal structure can be used to calculate the solid solution compositions.

The dissolved amount of the additives in ZrC matrix was calculated from the differences in the lattice parameters between the isolated monocarbides of ZrC (4.6970 Å), VC (4.300 Å), NbC (4.469 Å) and TaC (4.454 Å) and the sintered ZrC ceramics with 10 vol% VC, NbC and TaC additives. The results listed in Table 2 show that the lattice parameters of ZrC with 2.5 vol%, 5 vol% and 10 vol% additions at 1900 °C remained constant, which indicates that only about 1.3 vol% VC was dissolved in the ZrC matrix. These results show that the solubility limit of VC in ZrC at 1900 °C is around 1.3 vol% (1.8 mol%) and 2.81 vol% (3.80 mol%) at 2000 °C, which agrees with the theoretical value in the ZrC–VC phase diagram (shown in Fig. 1). According to the VC solubility limit, the dissolved VC in ZrC has reached its solubility limit with 2.5–10 vol% additions VC sintered at 1900 °C for 1 h and the excessive VC was observed as the second phase (Fig. 4a).

NbC and TaC form solid solutions with ZrC differently from VC. The phase diagrams at thermal equilibrium indicate that ZrC can theoretically form unlimited solid solution with NbC or TaC at the sintering temperatures (1900–2000 °C). However, the experimental solid solubility of NbC or TaC in ZrC is only 0.79 vol% NbC and zero TaC. The XRD patterns of the ZrC with NbC and TaC at 1900 °C also show that a series of Zr(Nb)C solid solutions formed, and the ZrC XRD peaks were broadened. Ta dissolution into the ZrC lattice was not detectable. The solubility results of both NbC and TaC in ZrC reported above are in conflict with the values shown on the phase diagrams (Fig. 1b and c). This is because the formation of solid solution under the dynamic diffusion rate could not complete or be detected during the isothermal hold times at the sintering temperature (1900 °C). When the sintering temperature rose to 2000 °C, most of the NbC or TaC dissolved in ZrC to form $Zr_{0.896}Nb_{0.104}C$ and $Zr_{0.895}Ta_{0.105}C$, which was verified by XRD patterns in Fig. 4d and f, as well as the lattice parameter in Table 2. It is important to note that formation of the limited solid solution of VC in ZrC finished at 1900 °C for 1 h, but solid solution of NbC in ZrC started to form at 1900 °C, and TaC dissolution in ZrC started

Table 2
Lattice parameters of ZrC and the calculated solution content with MC (M = V, Nb and Ta) additives sintered at different temperature.

Compositions	VC molar fraction (mol%)	Sintering conditions	Lattice parameters (Å) (±0.0002)	Calculated solid solubility (mol%)	Calculated solid solubility (vol%)	Solid solution formula
ZrC + 10 vol% VC	13.5	2000 °C–1 h	4.6865	3.80	2.81	$Zr_{0.962}V_{0.038}C$
ZrC + 10 vol% VC	13.5	1900 °C–1 h	4.6898	1.81	1.34	$Zr_{0.982}V_{0.018}C$
ZrC + 10 vol% NbC	11.24	1900 °C–1 h	4.6945	1.10	0.79	$Zr_{0.989}Nb_{0.011}C$
ZrC + 10 vol% NbC	11.24	2000 °C–1 h	4.6733	10.39	9.24	$Zr_{0.896}Nb_{0.104}C$
ZrC + 10 vol% TaC	11.56	1900 °C–1 h	4.6969	0	0	$Zr_{1.0}C$
ZrC + 10 vol% TaC	11.56	2000 °C–1 h	4.6715	10.49	9.07	$Zr_{0.895}Ta_{0.105}C$
ZrC + 1.0 vol% VC	1.4	1900 °C–1 h	4.6911	1.49	1.0	$Zr_{0.985}V_{0.015}C$
ZrC + 2.5 vol% VC	3.5	1900 °C–1 h	4.6897	1.84	1.31	$Zr_{0.982}V_{0.018}C$
ZrC + 5.0 vol% VC	6.9	1900 °C–1 h	4.6899	1.79	1.30	$Zr_{0.982}V_{0.018}C$
ZrC + 2.5 vol% VC	3.5	1900 °C–0 h	4.6919	1.28	0.91	$Zr_{0.987}V_{0.013}C$

after 1900 °C. The solid solution formation temperature is in the order $T_{VC} < T_{NbC} < T_{TaC}$. The kinetic rate of ZrC solid solution formation with MC increased in the order of TaC < NbC < VC.

The MC additives, having different kinetic rates of solid solution formation with ZrC matrix as reported above, determine the different effects on the densification of ZrC. VC forms a limited solid solution with ZrC matrix and can quickly reach its solubility limit at 1900 °C, so VC additive can promote the sintering of ZrC at the sintering temperatures of 1900 °C and 2000 °C. However, NbC and TaC cannot form or complete formation of unlimited solid solution with ZrC, under their dynamic diffusion rates at 1900 °C. Although increasing the sintering temperature to 2000 °C can promote the dissolution of NbC and TaC in ZrC during 1 h holding, the benefit to densification is limited. According to the phase diagrams shown in Fig. 1, the melting point of ZrC–VC solid solution is lower than that of pure ZrC and decreases with the increase of VC content, while the opposite trend occurs for NbC and TaC. The higher melting point indicates the stronger bond energy. The bond energy of V–C, Zr–C, Nb–C, is 427 ± 24, 561 ± 25, 569 ± 13 kJ/mol, respectively. [25] So the chemical bonds would be stronger in Zr–Nb–C solid solution than in Zr–V–C one. The stronger chemical bonds of Zr–Nb–C and Zr–Ta–C solid solutions resulted in poorer sintering ability than was expected in Zr–V–C solid solution, even though the Ta–C bond energy is not available. This may be the reason why the sintered density of ZrC with 10 vol% MC additives at 2000 °C is in the order of VC > NbC > TaC.

Based on the analysis reported above, VC is a more effective additive for ZrC sintering, compared with NbC and TaC. For 1.0 vol% addition, all the added VC dissolved in the ZrC lattice (although this composition sample showed only 86% since the dissolved VC was insufficient to disorder the ZrC lattice and enhance the densification). ZrC with 2.5 vol% VC was hot-pressed to 1900 °C without holding and the solid solubility was 0.91 vol% (1.28 mol%) as shown in Table 2. With the holding time increased to 1 h, the solid solubility reached the solubility limit (1.8 mol%). At the same time, the relative density also increased from 83.4% for no holding to 98% for 1 h holding. Therefore, the solid solution formation is a diffusion process which accompanies the densification process. The solid solubility of VC up to the solubility limit provided the maximum sintering density of 98%.

3.3. Microstructures

Microstructures of the pure ZrC ceramics and those with MC additives are compared in Fig. 7. The ZrC with 10 vol% VC has homogeneous microstructure with a small amount of porosity. The inset image in Fig. 7b shows that the grain size of ZrC is larger than that of other compositions and micropores trapped within the grains. In contrast, pure ZrC and that with NbC and TaC have almost no grain growth and the grain sizes are comparable to the starting ZrC powders. On the other hand, different content of VC resulted in different porosity in the ZrC ceramics (Fig. 8). The ZrC sample with 1.0 vol% VC has a porosity of

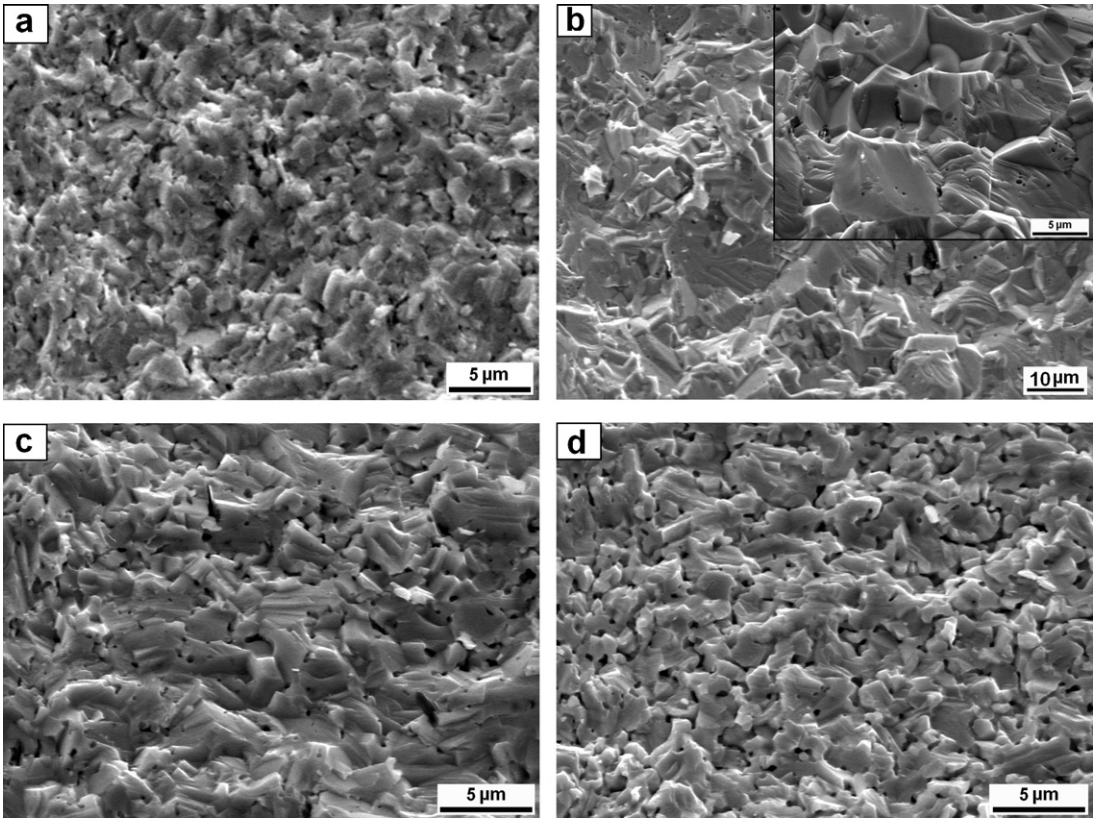

Fig. 7. SEM images of pure ZrC (a), ZrC with 10 vol% VC (b), 10 vol% NbC (c), and 10 vol% TaC (d) sintered at 2000 °C. The inset in b shows higher magnification image.

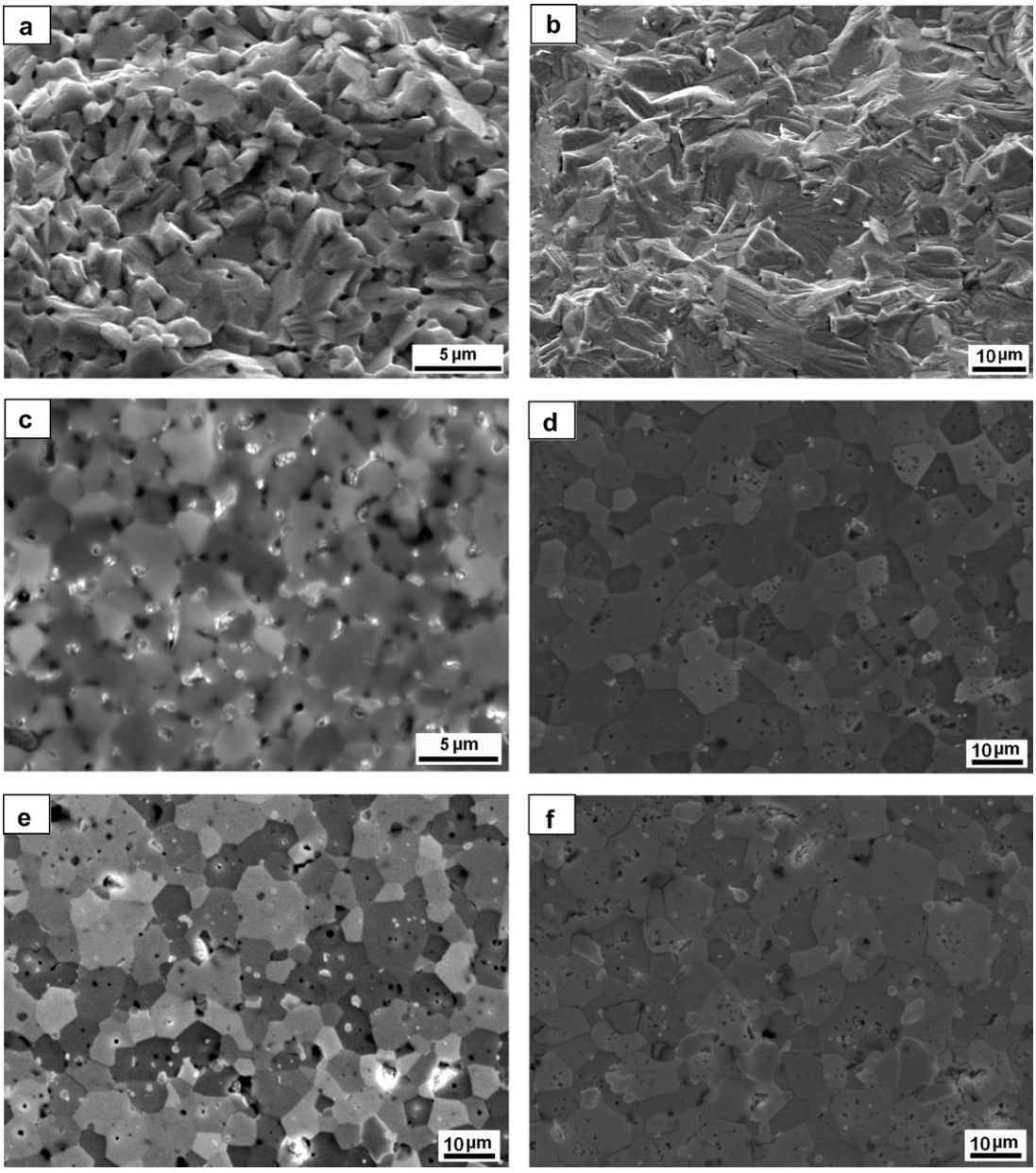

Fig. 8. Secondary electron images of fracture surface of ZrC with (a) 1.0 vol% VC, (b) 2.5 vol% VC, and polished surface after acid etching (c) 1.0 vol% VC, (d) 2.5 vol% VC, (e) 5.0 vol% VC, (f) 10 vol% VC.

6.7% and pores can be observed clearly (Fig. 8a). When VC content increased up to 2.5 vol% or higher, the pores could barely be observed (Fig. 8b) at 1900–2000 °C, which testified that VC at this content level was an effective additive to aid the densification of ZrC.

Fig. 8c–f shows the acid etched polished surfaces of ZrC with 1.0–10 vol% VC sintered at 1900 °C for 1 h. The average grain size of ZrC with 1.0 vol% VC was 2.4 ± 0.6 μm, whereas that of ZrC with 2.5–10 vol% VC was about 7.0–8.2 μm. The VC addition promoted the densification by forming a limited solid solution, but also resulted in the grain growth caused by the grain boundary diffusion.[15] There was no obvious grain growth in ZrC ceramics with NbC or TaC addition because the formed solid solutions of $Zr_{0.896}Nb_{0.104}C$ and $Zr_{0.895}Ta_{0.105}C$ have much stronger chemical bond than $Zr_{0.962}V_{0.038}C$ and their grain boundary diffusion energy was also much higher than that of $Zr_{0.962}V_{0.038}C$.

4. Conclusion

The ZrC ceramics with MC (M = V, Nb, and Ta) additives were prepared by hot-pressing at 1900 °C and 2000 °C. The solid solution formation of MC in ZrC, including solubility limit, forming temperature, kinetic rate and their effects on ZrC densification were studied by means of XRD, lattice parameter measurement and microstructure observation. The following conclusion can be drawn regarding the densification of ZrC with MC additions:

(1) NbC and TaC formed unlimited solid solution with ZrC, but VC formed a limited solid solution with ZrC. The solubility limit of VC was 1.3 vol% (1.8 mol%) at 1900 °C and 2.8 vol% (1.8 mol%) at 2000 °C.
(2) The solid solution of VC in ZrC formed early at 1900 °C, but solid solution of NbC in ZrC started at 1900 °C. TaC dissolution in ZrC started after 1900 °C. The temperature of solid solution formation is in the order $T_{VC} < T_{NbC} < T_{TaC}$. The kinetic rate of ZrC solid solution formation increased in the order TaC < NbC < VC. VC is the optimum additive because it has a lower temperature and faster rate than NbC and TaC to form limited solid solution with ZrC to promote the densification.
(3) The amount of dissolved VC also affected the densification and grain growth behavior of ZrC. When the VC addition was below the solid solubility limit (about 1.30 vol%), VC was not enough to effectively enhance the densification. ZrC with 2.5 vol% VC or above this level had relative density up to 98% at 1900 °C. Meanwhile, the ZrC with VC(>2.5 vol%) ceramics had grain growth, with grain size up to 7.0–8.2 μm, which is higher than that of ZrC with NbC or TaC additives.

Acknowledgements

Financial supports from the National Natural Science Foundation of China (No. 51002168) and (No. 91026008) are greatly appreciated. The authors appreciate Shi C. Zhang for many helpful discussions.

References

1. Upadhya K, Yang JM, Hoffman WP. Materials for ultrahigh temperature structural applications. *Am Ceram Soc Bull* 1997;**76**:51–6.
2. Sciti D, Guicciardi S, Nygren M. Spark plasma sintering and mechanical behaviour of ZrC-based composites. *Scripta Mater* 2008;**59**: 638–41.
3. Zou L, Wali N, Yang J-M, Bansal NP. Microstructural development of a C_f/ZrC composite manufactured by reactive melt infiltration. *J Eur Ceram Soc* 2010;**30**:1527–35.
4. Ogawa T, Ikawa K. High-temperature heating experiments on unirradiated ZrC-coated fuel particles. *J Nucl Mater* 1981;**99**:85–93.
5. Vasudevamurthy G, Knight TW, Roberts E, Adams TM. Laboratory production of zirconium carbide compacts for use in inert matrix fuels. *J Nucl Mater* 2008;**374**:241–7.
6. Gosset D, Dolle M, Simeone D, Baldinozzi G, Thome L. Structural evolution of zirconium carbide under ion irradiation. *J Nucl Mater* 2008;**373**:123–9.
7. Nosek A, Conzen J, Doescher H, Martin C, Blanchard J. Thermomechanics of candidate coatings for advanced gas reactor fuels. *J Nucl Mater* 2007;**371**:288–303.
8. Ryu HJ, Lee YW, Il Cha S, Hong SH. Sintering behaviour and microstructures of carbides and nitrides for the inert matrix fuel by spark plasma sintering. *J Nucl Mater* 2006;**352**:341–8.
9. Barnier P, Brodhag C, Thevenot F. Hot-presing kinetics of zirconium carbide. *J Mater Sci* 1986;**21**:2547–52.
10. Bulychev VP, Andrievskii RA, Nezhevenko LB. The sintering of zirconium carbide. *Powder Metall Met Ceram* 1977;**16**:273–6.
11. Samsonov GV, Koval'chenko MS, Petrykina RY, Naumenko VY. Hot pressing of the transition metals and their carbides in their homogeneity regions. *Powder Metall Met Ceram* 1970;**9**:713–6.
12. Wang XG, Guo WM, Kan YM, Zhang GJ, Wang PL. Densification behavior and properties of hot-pressed ZrC ceramics with Zr and graphite additives. *J Eur Ceram Soc* 2011;**31**:1103–11.
13. Gendre M, Maître A, Trolliard G. A study of the densification mechanisms during spark plasma sintering of zirconium (oxy-)carbide powders. *Acta Mater* 2010;**58**:2598–609.
14. Gendre M, Maître A, Trolliard G. Synthesis of zirconium oxycarbide (ZrC_xO_y) powders: Influence of stoichiometry on densification kinetics during spark plasma sintering and on mechanical properties. *J Eur Ceram Soc* 2011;**31**:2377–85.
15. Zhang XH, Hilmas GE, Fahrenholtz WG, Deason DM. Hot pressing of tantalum carbide with and without sintering additives. *J Am Ceram Soc* 2007;**90**:393–401.
16. Wang XG, Guo WM, Zhang GJ. Pressureless sintering mechanism and microstructure of ZrB_2–SiC ceramics doped with boron. *Scripta Mater* 2009;**61**:177–80.
17. Landwehr SE, Hilmas GE, Fahrenholtz WG, Talmy IG. Processing of ZrC–Mo cermets for high-temperature applications, part I: chemical interactions in the ZrC–Mo system. *J Am Ceram Soc* 2007;**90**:1998–2002.
18. Huang SG, Vanmeensel K, Van der Biest O, Vleugels J. Binderless WC and WC–VC materials obtained by pulsed electric current sintering. *Int J Refract Met Hard Mater* 2008;**26**:41–7.
19. Hu CF, Sakka Y, Jang B, Tanaka H, Nishimura T, Guo S, et al. Microstructure and properties of ZrB_2–SiC and HfB_2–SiC composites fabricated by spark plasma sintering (SPS) using $TaSi_2$ as sintering aid. *J Ceram Soc Jpn* 2010;**118**:997–1001.
20. Gusev AI, Rempel AA, Magerl AJ. *Disorder and order in strongly monstoichiometric compounds*. Berlin: Springer; 2001.
21. ACerS-NIST Phase Equilibria Diagram, CD-ROM Database, Version 3.1; 2005.
22. Johansson KE, Palm T, Werner PE. An automatic microdensitometer for X-ray powder diffraction photographs. *J Phys E: Sci Instrum* 1980;**13**: 1289–91.
23. Werner PE. A Fortran program for least-squares refinement of crystal-structure cell dimensions. *Arkiv fur Kemi* 1964;**31**:513–6.
24. Rempel' AA. Atomic and vacancy ordering in nonstoichiometric carbide. *Phys Usp* 1996;**39**:31–56.
25. Lide David R. *CRC handbook of chemistry and physics*. 88th ed. CRC Press; 2007-2008.